ELSEVIER

Catalysis Communications 1 (2000) 25–31

CATALYSIS COMMUNICATIONS

www.elsevier.nl/locate/catcom

Raman and kinetic evidence of NO_2^+ ion in solid acid catalysts

Nunziata Clara Marziano [a,*], Lucio Ronchin [a], Sabina Ronchin [b], Maurizio Ferrari [c]

[a] *INFM and Chemistry Department, University of Venice, DorsoDuro 2137, 30123 Venice, Italy*
[b] *INFM and Department of Physics, University of Trento, Sommarive 14, 38050 Trento, Italy*
[c] *CNR – CeFSA, Sommarive 14, 38050 Trento, Italy*

Received 31 July 2000

Abstract

Samples of H_2SO_4/SiO_2 loaded with HNO_3 and analysed by Raman spectroscopy exhibit the band of the NO_2^+ ion, which is formed by the protonation–dehydration equilibrium of HNO_3 in strong acidic media. The effectiveness of NO_2^+ as a nitrating species is tested in the nitration of aromatic compounds towards substrates with high acid requirements for the conversion reagents–products. The acidic properties of the acid systems used as catalysts are also described, and the thermodynamic parameters related to the acid–base proton transfer process are discussed.

Keywords: NO_2^+ ion; Solid acid catalysts; Nitration; Acidity

1. Introduction

Acidity and catalytic performance are the key parameters of interest for economic design and practical applications in the field of acid-catalysed reactions. A number of studies in liquid and solid phase [1–3] have attempted to obtain the details which need to be known in order to carry out a reaction under optimal experimental conditions.

In the present paper, the catalytic properties of supported acids (H_2SO_4/SiO_2) have been tested in the nitration of aromatic compounds (Scheme 1), chosen as the model of a reaction with strong acid requirements for the conversion reagents–products [4–6]. Evidences by Raman measurements are also given for the existence of the NO_2^+ ion in the solid phase. This ion, recognised as a nitrating species, is formed from nitric acid by equilibrium (2) under a suitable acidity of medium and is present in spectroscopically detectable amounts in very strong acid systems [6–8].

$$Ar + HNO_3 + H^+ \rightarrow ArNO_2 + H_2O \quad (1)$$

$$HNO_3 + H^+ \rightleftharpoons NO_2^+ + H_2O \quad (2)$$

The results have been compared to those obtained in aqueous phases, where the nitration rates of a large number of compounds [4–6] and the equilibrium constant of the NO_2^+ ion are now available [6–8]. For an improved understanding of the phenomena governing the catalytic processes in different media, the acid strength of the acid catalysts has also been estimated by a procedure where the variations of the activity coefficients of

* Corresponding author. Fax: +39-41-257-8517.
E-mail address: marziano@unive.it (N.C. Marziano).

1566-7367/00/$ - see front matter
PII: S1566-7367(00)00004-2

the species and the acid–base interactions are taken into account [6,9,10].

2. Experimental

2.1. Catalyst preparation

Purified samples of commercially available silica gel (GRACE, 90 μm average particle size) were obtained by washing the material with aqueous solutions of perchloric acid, then with distilled water before drying at 105°C in a stream of N_2. Weighted amounts of the resulting solid and aqueous sulphuric acid of appropriate concentrations were mixed under stirring, and the supernatant solution was removed by filtration after ~1 h. The catalyst was dried at 105°C in a stream of N_2 for 72 h.

2.2. Catalyst characterisation

The catalysts have been characterised by different techniques:

(a) The acid in the solids after impregnation was determined by automatic potentiometric titrations against standard solutions of NaOH.

(b) BET surface area (SA), pore size distribution (BJH model) and total pore volume (relative pressure of $p/p_0 = 0.98$) were determined by N_2 adsorption and desorption at 94 K using an automatic adsorption unit (Micromeritics ASAP 2010C).

(c) MicroRaman spectra of the catalysts were recorded by an optical microscope in a backscattering configuration (Olimpus BHSM-L-2 model) using an argon-ion laser operating at 488 nm, vertically polarised and kept at constant power (100 mW). The spectra were recorded by analysing the scattered light. The signal was collected by a Jobin Yvon U 1000 double monochromator and analysed by a photon-counting system. A resolution of 4 cm^{-1} was employed for all measurements.

(d) XPS measurements of the catalyst were made using pyridine chemisorption and investigation of the N_{1s} XPS band [11]. XPS peak areas of Si (2p) and S (2p) were also analysed.

2.3. Raman measurements of adsorbed nitric acid

Nitric acid solutions in dichloromethane (0.2–1.5 M) prepared by dried solvent and fresh distilled nitric acid were used. A small amount of the catalysts was added to the solutions, contained in a quartz cell kept at 25°C. Samples with 3–5 mmol $H_2SO_4/g_{catalyst}$ were analysed. The Raman spectra were in the standard 90° geometry using an argon-ion laser operating at 488 nm, vertically polarised and kept at constant power (100 mW). The spectra were recorded by analysing the scattered light with polarisation parallel to that of the exciting beam. The signal was collected by a Jobin Yvon U 1000 double monochromator, and analysed by a photon-counting system. A resolution of 4 cm^{-1} was employed for all measurements. A strong luminescence of the samples was the main experimental difficulty, which was strongly reduced by the addition of nitric acid.

2.4. Kinetics measurements of aromatic nitration

The kinetics measurements were performed in a well-stirred UV cell containing weighed samples of the catalyst, aromatic (Ar) and distilled nitric acid in dry dichloromethane.

The experimental conditions used were: [Ar] 10^{-5} (M), [HNO_3] between 5×10^{-3} and 3×10^{-2} (M), samples of catalyst (0.25 g) with different acid loadings (1.93, 3.15, 3.31, 4.15, 4.25, 5.07 mmol $H_2SO_4/g_{catalyst}$). The cell was kept at 25°C, and the change of absorbance with time at selected wavelengths was followed for the nitration of nitrobenzene, *o*-, *m*- and *p*-chloronitrobenzenes and 4-chloro-3-nitrotoluene. Good linear pseudo-first-order kinetic plots (r_0 values) were obtained in all cases, and second-order rate constants ($k_{2obs}/dm^3/mol\ s$) were calculated from the stoichiometric concentrations of nitric acid.

3. Results and discussions

3.1. Analysis of the catalytic material

In Table 1, the dependence between the concentration of the impregnating solution and the

Table 1
Properties of the catalyst at different acid loadings

H_2SO_4 wt%[a]	H_2SO_4 mmol/g catalyst[b]	BET surface area[c]	Total pore volume[d]
0	0	364	1
10	3.8	291	0.88
18	6.3	214	0.71
21	6.6	182	0.67
28	8.3	136	0.36
30	8.7	108	0.33
38	10.1	80	0.18

[a] Acid % composition in the starting solution.
[b] Acid in the solid catalyst.
[c] BET surface area m^2/g.
[d] Total pore volume N_2 adsorption at $p/p_0 = 0.98$ ml/g.

properties of the catalyst is reported. For instance, a progressive decrease of surface area and total pore volume is observed as the sulphuric acid loading increases. On the contrary, pore size distribution exhibits a constant average diameter of ca. 8 nm. An excess of water allows the complete leaching of sulphuric acid without a change in the silica framework. It appears on the control of the resulting material, whose values of surface area and porosity are analogous to the ones observed in the starting sample.

Details related to type of acid site are obtained by XPS and Raman measurements. On analysis by pyridine chemisorption and investigation of the N_{1s} XPS band, the samples exhibit a single peak at 401 eV due to the presence of Broensted acid sites [11]. On analysis by the XPS peak areas of Si (2p) and S (2p), the Si/S ratios are found to be proportional to the amount of sulphuric acid added to the silica gel.

The microRaman spectrum of the catalyst loaded with 4.65 mmol $H_2SO_4/g_{catalyst}$ is shown in Fig. 1, where bands at 420, 587, 902, 981 and 1044 cm^{-1} are observed. The band at 981 cm^{-1} of SiO_2 (SiOH stretching mode of isolated surface silanol species) [12] and the band at 1044 cm^{-1} of bisulphate ion [13] can be easily recognised.

All the previous results suggest that (i) the strong Broensted acid sites observed on the catalyst are due to the added sulphuric acid; (ii) the isolated silanol group are due to incomplete coverage of the surface; (iii) the sulphuric acid fills the pore in proportion to the amount of the acid loading. The addition decreases pore volume and surface area without changing the pore size distribution.

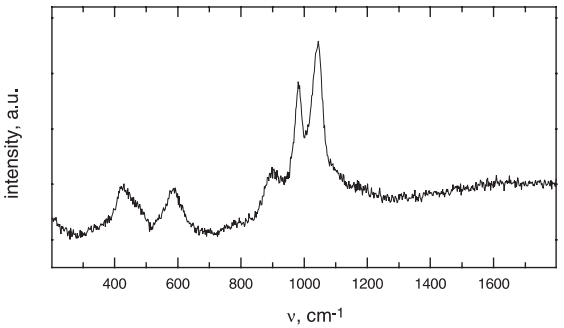

Fig. 1. MicroRaman spectrum of H_2SO_4/SiO_2 at 25°C. Sample with 4.65 mmol $H_2SO_4/g_{catalyst}$.

3.2. Equilibria of the nitrating species

In Fig. 2, the Raman spectra of the catalyst loaded with nitric acid and of the standard mixtures used for comparison are reported, together with the variations observed by changing the experimental conditions. The spectral behaviour shows essentially that the conversion of nitric acid to nitronium ion according to equilibrium (2) is extremely sensitive to the acidic properties of the surface. Thus, the band at 1400 cm^{-1} of NO_2^+ ion and the band at 1300 cm^{-1} of undissociated nitric acid, already assigned by Raman studies [7,8], have been observed in dry acid samples (Fig. 2(c)). The electrophilic species disappears by the addition of water (Fig. 2(d)). In the supernatant

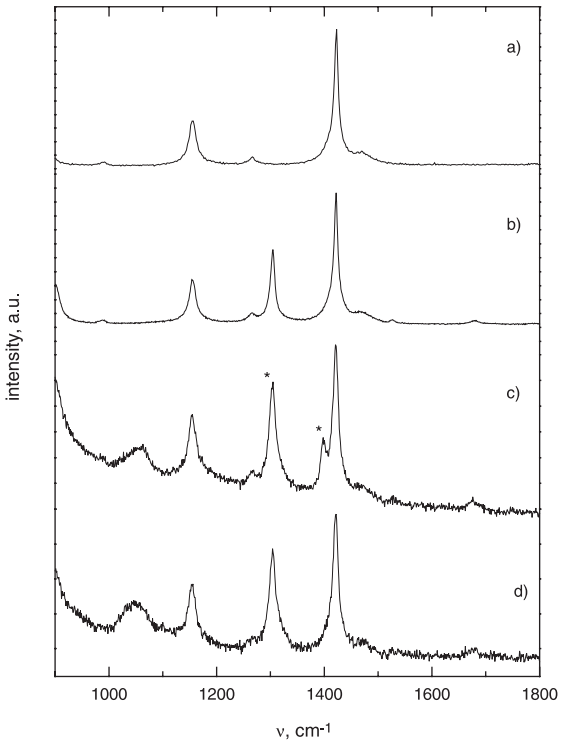

Fig. 2. Raman spectra at 25°C of: (a) dichloromethane; (b) dichloromethane + nitric acid ($[HNO_3] = 1.5$ M, total volume = 1.8 ml); (c) 0.5 g of catalyst (4.65 mmol $H_2SO_4/g_{catalyst}$) added with (b) sample; (d) water (20 μl) added to (c) sample.

solution, only molecular nitric acid has been detected with a spectral trend analogous to the one recorded in liquid and solid phase using unsupported dried silica (Fig. 2(b)).

The Raman results suggest that the acid–base equilibria between HNO_3, H_2SO_4 and SiO_2 occur over the surface layers of the samples. Additional experimental observations support analogous conclusions. Using XPS measurements, for instance, the binding energies (BEs) of N_{1s}, Si_{2p} and S_{2p} of a catalyst containing 2.52 mmol $H_2SO_4/g_{catalyst}$ and different amounts of isopropyl nitrate show a linear relationship in the plots Si/N and S/N vs. the amount of the nitrating agent added to the sample. Isopropyl nitrate was used as the precursor of the effective NO_2^+ ion.

The spectral behaviour of nitric acid in the solid catalyst appears to be very similar to that observed in concentrated aqueous solutions of strong acids [7]. Indeed, in the range 82–92 wt% H_2SO_4, the conversion $HNO_3 \rightarrow NO_2^+$ parallels the acidity of the solvent, and the Raman spectra of the solutions exhibit the band characteristic of the molecular and ionic species. In acidic media >92 wt%, the ionisation of HNO_3 to NO_2^+ is virtually complete. Below 82 wt% the NO_2^+ band disappears, and a change of the $\log[NO_2^+]/[HNO_3]$ ratio between 10^{-12} and 10^{-2} has been estimated in going from 50 to 80 wt% H_2SO_4 [6]. Substitution of trifluoromethanesulphonic acid (TFMSA) for sulphuric acid in the Raman studies of the NO_2^+ ion [8] induces a spectral behaviour analogous to that observed in H_2SO_4, both H_2SO_4 and TFMSA, between 80 and 100 wt%, being substantially stronger acids than HNO_3 [14,15].

3.3. Acid-catalysed nitration

Samples of H_2SO_4/SiO_2 with different acid loading have recently been tested for a synthetic route of aromatic nitrocompounds [16]. The results show that good yields of products (>95%) can be obtained at 25°C using commercial nitric acid as nitrating agent and supported catalysts with acid loading to be modified in accordance to the reactivity of the aromatic substrates. The knowledge of substituent effects on aromatic compounds is one of the most important aspects of the broader question of reactivity in electrophilic reactions, and in Table 2, the k_2° rate constants of some activated and deactivated compounds in aqueous sulphuric acid are reported. The k_2° values are independent of medium acidity and are related to the stoichiometric concentration of nitric acid and to the effective concentration of NO_2^+ by Eq. (3) [6,17]

$$k_{2obs}[Ar]_{st}[HNO_3]_{st} = k_2^\circ[Ar][NO_2^+]. \quad (3)$$

It can be seen that, for nitrobenzene or substituted nitrobenzenes, less reactive than benzene by a factor between 10^6 and 10^9, samples of catalyst with high acid loading occur. According to the reactivities of the substrates and the spectroscopic observations obtained by Raman in the solid phase, kinetic measurements of nitrobenzenes over H_2SO_4/SiO_2 have been performed using an-

Table 2
Second-order rate constants (log k_2°/dm^3 mol^{-1} s^{-1}) and activation energies (E_a°/kcal mol^{-1}) for nitration in aqueous sulfuric acid at 25°C

Compounds	log k_2°[a]	Relative rates[b]	E_a°[c]
Mesitylene	7.87	1.82	7.3
Toluene	7.44	1.39	8.4
Benzene	6.05	0.00	9.2
Chlorobenzene	5.05	−1.00	11.1
4-chloro-3-nitrotoluene	0.15	−5.90	
o-chloronitrobenzene	−0.60	−6.65	15.8
Nitrobenzene	−1.10	−7.15	
m-chloronitrobenzene	−1.75	−7.80	
p-chloronitrobenzene	−2.10	−8.15	16.9

[a] Estimated by Eq. (3). [NO_2^+] determined by the equilibrium values: $pk_{NO_2^+} = -17.3, n_{NO_2^+}, n_{NO_2^+} = 2.46$ (from Ref. [6]).
[b] Relative rates $= \log(k^{\circ}_{2(PhX)}/k^{\circ}_{2(PhH)})$.
[c] E_a° values determined by the k_2° rate constants.

hydrous nitric acid and catalysts with H_2SO_4 between 2 and 5 mmol acid/$g_{catalyst}$.

Under these experimental conditions, nitrobenzene, *o*-, *m*-, *p*-chloronitrobenzenes and 4-chloro-3-nitrotoluene can be easily nitrated, and the kinetic behaviour observed in the nitration of *o*-chloronitrobenzene is reported in Fig. 3. For a better understanding of the results the k_{2obs} (see Fig. 3(a)) and the k^*_{2obs} (see Fig. 3(b)) rate constants defined, respectively, by Eqs. (4) and (5) have been determined. All the values have been obtained from the pseudo-first-order kinetics plots (r_0 values) by taking into account the stoichiometric concentration of nitric acid and the acid loadings, also corrected for the variation of surface area by a factor f. The k^*_{2obs}, within the limits of experimental errors, are found to be almost independent of the acid loading of the catalysts.

$$k_{2obs} = r_0/[HNO_3]_{st} \times [Acid], \quad (4)$$

$$k^*_{2obs} = r_0/[HNO_3]_{st} \times [Acid] \times f, \quad (5)$$

where $f = SA_{cat}/SA_{SiO_2}$.

The different trend of (k_{2obs}) and (k^*_{2obs}) suggests that the nitronium ion on the surface is the effective nitrating agent which interacts with the aromatic by rate values according to the reactivity of the substrate. This mainly appears from the results in Table 3, where the k^*_{2obs} rate constants of different substituted nitrobenzenes are reported. The comparison in Table 3 between k^*_{2obs} and k_2° values determined for analogous compounds in aqueous solutions is also of interest. The linear relationship

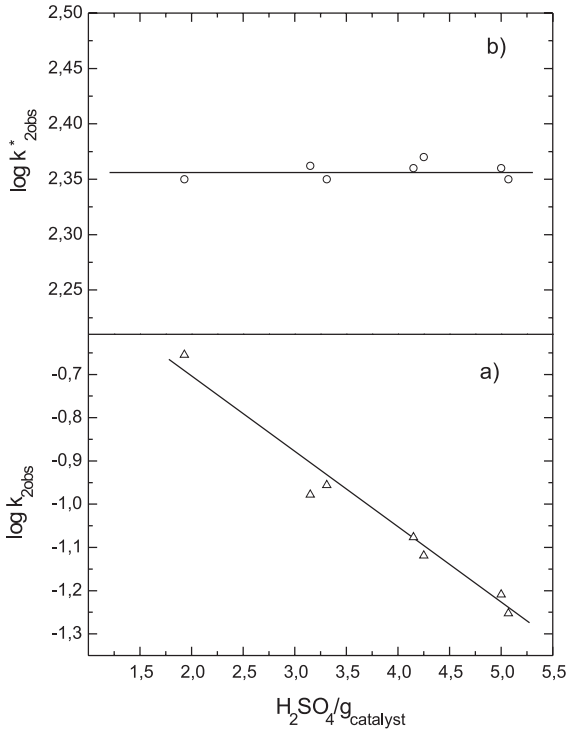

Fig. 3. k_{2obs} and k^*_{2obs} rate constant vs. the acid loading of the catalyst in the nitration of *o*-chloronitrobenzene.

observed between ($k^*_{2obs(X-PhNO_2)}/k^*_{2obs(PhNO_2)}$) values obtained in solid-phase nitration and ($k^{\circ}_{2(X-PhNO_2)}/k^{\circ}_{2(PhNO_2)}$) values obtained in aqueous sulphuric acid nitration strongly suggests that the proton transfer process and the reactivity of the compounds under investigation are analogously

Table 3
Second-order rate constant for nitration at 25°C in H_2SO_4/SiO_2 (log k^*_{2obs}/dm^3 mol^{-1} s^{-1}) and in aqueous H_2SO_4 (log k°_2/dm^3 mol^{-1} s^{-1})

Compounds	log k^*_{2obs}[a]	Relative rates[b]	log k°_2[c]	Relative rates[d]
	H_2SO_4/SiO_2		H_2SO_4(aq)	
4-chloro-3-nitrotoluene	2.88	0.90	0.15	1.25
o-chloronitrobenzene	2.36	0.38	−0.60	0.50
Nitrobenzene	1.98	0.00	−1.10	0.00
m-chloronitrobenzene	1.36	−0.62	−1.75	−0.65
p-chloronitrobenzene	1.17	−0.80	−2.10	−1.00

[a] Estimated at 4.15 mmol $H_2SO_4/g_{catalyst}$ by Eq. (5).
[b] Relative rates $= \log(k^*_{2obs\ (X\text{-}PhNO_2)}/k^*_{2obs\ (PhNO_2)})$ in solid phase nitration.
[c] Estimated by Eq. (3).
[d] Relative rates $= \log(k^\circ_{2(X-PhNO_2)}/k^\circ_{2(PhNO_2)})$ in aqueous phase nitration.

related in both phases [17]. However, in the comparison between liquid and solid, it is also significant to note that the k^*_{2obs} are higher by a factor of ca. 10^3 compared to the k°_2 values, due to a highly efficient proton transfer process in the solid acid catalyst. It represents a practical aspect of applicability of an inexpensive solid acid material instead of aqueous acid solutions.

3.4. Studies of proton transfer process in solid acids

It is well known [1–3] that the catalytic activity of solid acids depends on the 'surface acidity' of the sites. This is suggested by a number of studies over H_2SO_4/SiO_2 with different acid loading (i.e., 0.1–0.5 mmol $HA/g_{catalyst}$), using the protonation of weak bases (B) as a measure of the 'protonating ability' of a given acid (HA) towards a given base (B) [18–20]. The acid–base equilibrium (equilibrium (6)) involved in the acid–base process is described by thermodynamic equation (7)

$$B + H^+ \rightleftharpoons BH^+ \tag{6}$$

$$pK_{BH^+} = \log[BH^+]/[B] - \log[H^+] - \log(f_B f_{H^+}/f_{BH^+}). \tag{7}$$

From a practical point of view, the titration curves have been determined, and the $\log[BH^+]/[B]$ ratios of B have been analysed by Eq. (7), rewritten as (7′), where the activity coefficients of reagents and products are taken into account by Eq. (8) [21,22]. The activity coefficient term is of interest since acid–base interactions in non-ideal systems are involved [6,9,10].

$$pK_{BH^+} = \log[BH^+]/[B] - \log[H^+] + b[C_A], \tag{7′}$$

$$-\log(f_B f_{H^+}/f_{BH^+}) = b[C_A]. \tag{8}$$

This procedure allows us to obtain pK_{BH^+} and b values, related, respectively, to the intercept and slopes of the plots $(\log[BH^+]/[B] - \log[H^+])$ vs. $[C_A]$ ($[C_A]$ = acid concentration).

For 2-Cl-4-NO_2- and 2,4-di-Cl-6-NO_2-aniline as weak bases, the observed values are: $pK_{BH^+} = -0.90$ and -3.50; $b = 5.5 \times 10^4$ and 3.7×10^4.

The pK_{BH^+} values, equal to the previous estimates in $HClO_4/SiO_2$, CF_3SO_3H/SiO_2 [18–20] and aqueous solutions of H_2SO_4, $HClO_4$, CF_3SO_3H, CH_3SO_3H and HNO_3 [6,9,10], suggest that the solid catalysts exhibit one type of acid site and thermodynamic constants that can refer to water as standard state.

Strong acid–base interactions can be inferred from the slope values, higher by a factor of ca. 10^4–10^5, compared to the ones (n_{is}) observed in concentrated aqueous acid solutions. Indeed, in the latter acid systems, where a very large number of experimental data have been analysed [6,9,10], relationship (9) has been found to hold, and n_{is} values have been recognised as parameters related to the *energetic proton transfer process from* H^+A^- *to* BH^+A^- [6,9,10].

$$\log(f_B f_{H^+}/f_{BH^+}) = -n_{is}\log(f_A - f_{H^+}/f_{HA}). \tag{9}$$

The left- and the right-hand terms of Eq. (9) refer to the activity coefficient terms of thermodynamic equations (7) and (11), describing the protonation of the weak base and the dissociation

of a strong acid in concentrated aqueous acid solution (equilibria (6) and (10)).

$$HA \rightleftharpoons A^- + H^+ \tag{10}$$

$$pK_{HA} = \log[HA]/[A^-] - \log[H^+] - \log(f_A - f_{H^+}/f_{HA}). \tag{11}$$

It follows that:

(i) A reasonable description of the acid–base equilibria of solid acid catalysts can be obtained by a thermodynamic procedure analogous to the one applied in aqueous acid phases.

(ii) The protonating ability of an acid is characterised by the specific acid–base interactions of the acid–base pair under investigation and determined by the b or n_{is} value.

(iii) The high protonating ability of the solid materials is in agreement with the spectroscopic detection of the NO_2^+ ion. Moreover, the rate constants of the kinetic measurements are also consistent with the whole experimental observations.

References

[1] G.A. Olah, G.K. Surya Prakash, J. Sommer, Superacids, Wiley, New York, 1985.

[2] K. Tanabe, H. Hattori, T. Yamaguchi, T. Tanaka, Acid–Base Catalysis, VCH, New York, 1989.

[3] A. Corma, Chem. Rev. 95 (1995) 559.

[4] K. Schofield, Aromatic Nitration, Cambridge University Press, Cambridge, 1980.

[5] G.A. Olah, R. Malhotra, S.C. Narang, Nitration. Methods and Mechanisms, VCH, New York, 1989.

[6] N.C. Marziano, A. Tomasin, C. Tortato, J.M. Zaldivar, J. Chem. Soc. Perkin Trans. 2 (1998) 1973.

[7] M. Sampoli, A. DeSantis, N.C. Marziano, F. Pinna, A. Zingales, J. Phys. Chem. 89 (1985) 2864.

[8] N.C. Marziano, A. Tomasin, M. Sampoli, J. Chem. Soc. Perkin Trans. 2 (1991) 1995.

[9] N.C. Marziano, A. Tomasin, C. Tortato, P. Isandelli, J. Chem. Soc. Perkin Trans. 2 (1998) 2535.

[10] N.C. Marziano, C. Tortato, L. Ronchin, C. Bianchi, Catal. Lett. 56 (1998) 159.

[11] R.B. Borade, A. Adnot, S. Kaliaguine, J. Catal. 126 (1990) 6.

[12] B.A. Morrow, A.J. MacFarlan, J. Phys. Chem. 95 (1992) 1395.

[13] H. Chen, D.E. Irish, J. Phys. Chem. 75 (1971) 2672.

[14] N.C. Marziano, A. Tomasin, C. Tortato, Org. React. (Estonia) 30 (1996) 29.

[15] N.C. Marziano, A. Tomasin, C. Tortato, Org. React. (Estonia) 30 (1996) 39.

[16] J.M. Riego, Z. Sedin, J. Zaldivar, N.C. Marziano, C. Tortato, Tetrahedron Lett. 37 (1996) 513.

[17] N.C. Marziano, C. Tortato, L. Ronchin, F. Martini, C. Bianchi, Catal. Lett. 58 (1999) 81.

[18] N.C. Marziano, C. Tortato, Abdiqafar A. Sheikh-Osman, J. Riego, J.M. Zaldivar, Org. React. (Estonia) 30 (1996) 49.

[19] N.C. Marziano, C. Tortato, Abdiqafar A. Sheikh-Osman, J. Riego, J.M. Zaldivar, Org. React. (Estonia) 31 (1997) 87.

[20] Unpublished results.

[21] C.H. Rochester, Acidity Functions, Academic Press, London, 1970.

[22] N.C. Marziano, G. Cimino, R. Passerini, J. Chem. Soc. Perkin Trans. 2 (1973) 1915.